Inorganic Chemistry

pubs.acs.org/IC Article

Self-Assembly of Complementary Components Using a Tripodal Bismuth Compound: Pnictogen Bonding or Coordination Chemistry?

Shiva Moaven, Brandon T. Watson, Thomas J. Polaske, Brian M. Karl, Daniel K. Unruh, Nathan P. Bowling,* and Anthony F. Cozzolino*

Cite This: https://doi.org/10.1021/acs.inorgchem.1c01232 Read Online

ACCESS | Metrics & More | Article Recommendations | Supporting Information

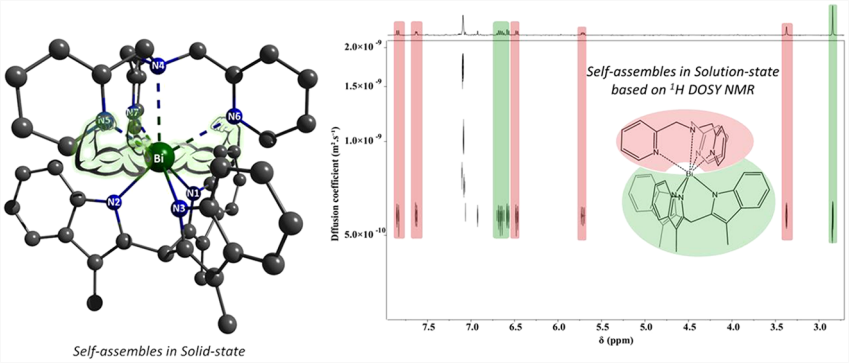

ABSTRACT: Triple pnictogen bonding refers to the ability of a pnictogen atom to engage in three simultaneous pnictogen bonds (PnBs) to a complementary partner through a single pnictogen atom. This supramolecular strategy was recently introduced as a unique facet of pnictogen bonding as compared to other named supramolecular interactions. Here, the ability of bismuth to participate in this phenomenon is demonstrated using $Bi((NC_9H_7)_3CH_3)$. The study reveals that Bi engages in stronger PnBs than the analogous Sb system. The results have been contrasted with Bi systems that form strong coordination bonds, and analysis of the electron density along the bond path reveals key differences. The solution behavior of these newly synthesized supramolecules were studied by PFGSE NMR spectroscopy and they are found to remain intact in solution. Molecular design strategies that allow for triple pnictogen bonding should find use in the fields of molecular recognition and crystal engineering.

■ INTRODUCTION

Pnictogen bonding (PnB) refers to the pnictogen-centered secondary bonding interactions (SBIs) that dominate the supramolecular chemistry of the heavy p-block elements.[1−4] In analogy to halogen (HaB) and chalcogen bonding (ChB), it can be defined as a net attractive interaction between an electrophilic region associated with a pnictogen element in a molecular entity (the donor) and a nucleophilic region in a molecular entity (the acceptor).[5,6] Pnictogen bonding categorizes a subset of interactions that are part of a continuum that ranges from nondirectional London dispersion interactions to more formal dative covalent bonds, and the exact boundaries are difficult to define.[7] Pnictogen bonding is widely observed in the solid-state structures of the heavier pnictogen atoms in their trivalent state but, when compared to halogen or chalcogen bonding, have not seen much purposeful employment as a supramolecular interaction. Some recent efforts to design functional molecules around pnictogen bonding include anion binding and transport,[8−12] noncovalent catalysis,[13−17] self-assembly of reversed bilayer vesicles,[18,19] and molecular recognition.[20−23] The paucity of examples may be a result of the differences in synthetic approaches and VSEPR geometries as compared with hydrogen and halogen bonding. An important corollary of these differences is the unique ability of pnictogen bond donors to engage in (up to) three simultaneous interactions as shown in Figure 1. Formation of three simultaneous PnBs involving three separate acceptors can lead to 2D or 3D self-assembly. When these interactions occur between a single donor and a single acceptor, the descriptor of a *triple pnictogen bond* can be applied and this triple PnB can be used to direct molecular recognition between two units with a high degree of specificity.

Received: April 21, 2021

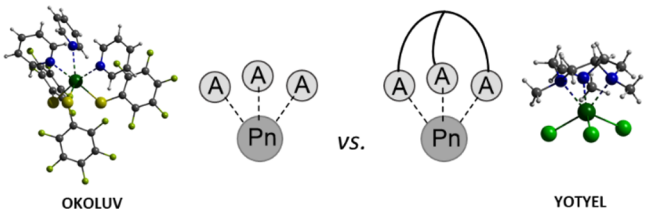

Figure 1. Comparison between three separate PnBs ($Bi(SC_6F_5)_3{\cdot}Py_3$: CSD code OKOLUV)[24] and triple pnictogen bonding ($BiCl_3{\cdot}Me_3[9]aneN_3$: CSD code YOTYEL).[25] The color of H, C, N, F, S, Cl, and Bi atom in this figure is white, gray, blue, yellow-green, yellow, green, and dark green, respectively.

It becomes pertinent to address the confusion that arises with bismuth about the terms pnictogen bond and coordination bond, particularly due to its classification as a metal. Traditionally, the chemistry of bismuth(III) that extends beyond a valency of three has been referred to as coordination chemistry and involves a continuum of distances and strengths. In this work, we use the term pnictogen bonding to specifically categorize the subset of these coordination bonds that occur opposite a pre-existing primary bond at a distance that clearly distinguishes them from primary bonds and involves little molecular reorganization. As such, they are functionally analogous to noncovalent interactions like hydrogen and halogen bonding. This way of categorizing these interactions is consistent with the lighter congeners and highlights the fact that they are comparable in strength to other supramolecular interactions like hydrogen and halogen bonding. To further clarify the usage of pnictogen bonding here, a few examples of molecular and coordination (mono and tricationic) compounds of Bi are shown in Figure 2.[23,26,27] Bismuth structures containing the tris-thioether ligand used by Benkő and Heift nicely illustrate these ideas (Figure 2).[20,23] When it binds to BiX_3 (X = Cl, Br, I), the Bi···S distances (3.047(9)-3.136(8) Å) are significantly longer than a covalent bond and occur nearly opposite to a pre-existing Bi−X bond. In the case of $Bi(OTf)_3$, the Bi−S distances match those of a covalent bond (2.749(9) Å) and they do not geometrically correlate with a pre-existing bond. It is useful to distinguish these two situations, the former weak coordination bonds being described here as PnBs and the latter as coordination bonds. The other implication of these classifications is a difference in strength regime, the former behaving more like a noncovalent interaction and the latter more like a covalent bond. While there is no hard and fast dividing line between bonds that are molecular in nature and those that behave more like a supramolecular interaction, generally covalent bond strengths are greater than 150 kJ/mol (with most greater that 200 kJ/mol) whereas, for instance, hydrogen bonds range in strength from 2 kJ/mol −170 kJ/mol.[28−30]

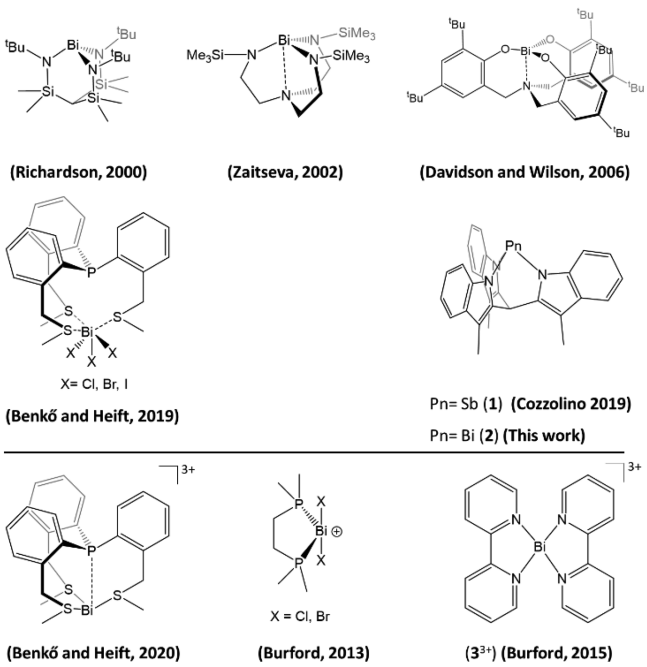

Figure 2. Examples of previously reported neutral Bi(III) compounds and the new compound **2** in this work (above the line). Examples of cationic Bi(III) coordination complexes (below the line).

In our recent study demonstrating the self-assembly directed by a triple PnB, we observed that the antimony pnictogen bond donor **1** (Figure 2) was capable of forming a triple PnB, but only when partnered with an appropriately designed triple PnB acceptor.[21] Computationally, it was found that the formation of each PnB decreased the strength of the subsequent pnictogen bond; significant negative cooperativity was associated with multiple PnB bond formation in this system. The origin of this was determined to be the increasing stereochemical activity of the pnictogen lone pair with each additional pnictogen bond, which in turn reduces the value of the positive electrostatic potential associated with the region where the PnB will form. Building positive cooperativity into the acceptor allowed for a strong and symmetrical triple pnictogen bond to form. This behavior is in contrast to that of antimony alkoxide cages that readily self-recognize and form three PnBs at each antimony.[31,32] A recent computational study that considers intramolecular PnBs identified a similar phenomenon.[33] For the alkoxide cages, no analogous bismuth alkoxide cage could be isolated, but density functional theory (DFT) calculations suggested that it should form the strongest pnictogen bonds. This is a result of three important considerations: 1) there is increased stereochemical inactivity of the bismuth lone pair, 2) the σ^*-orbitals involved in PnB formation are lower in energy, and 3) there is an increase in polarizability. From this it follows that a bismuth analogue (**2** in Figure 2) should not be as susceptible to negative cooperativity upon pnictogen bond formation and is therefore expected to be a more efficient triple PnB donor than **1**.

While examples of triple-pnictogen bonding with bismuth can be observed in crystal structures (see Benkő and Heift 2019 in Figure 2, for example),[20] no examples have been observed with tripodal bismuth compounds. Tripodal Bi(III) compounds that have been reported (Figure 2) either have bulky groups around the potential PnB sites or have a geometry that does not allow for ready formation of a PnB opposite to an existing primary bond.[34−36] In some cases, transannular Bi···N interactions are observed. While these are not necessarily PnBs, they reflect the Lewis acidity of the Bi center in these tripodal systems and are probably best characterized as coordination bonds.[34−36] Compound $\mathbf{3}^{3+}$ was selected as a good example of coordination bonding with bismuth(III) involving pyridyl groups and will be used in this study to contrast its bonding properties with those of compound **2**.

https://doi.org/10.1021/acs.inorgchem.1c01232
Inorg. Chem. XXXX, XXX, XXX−XXX

■ RESULTS AND DISCUSSION

Synthesis and Characterization of 2. Similar to the preparation of the antimony congener, **2** was prepared by treating 2,2′,2″-triskatylmethane, suspended in anhydrous benzene, with 1.1 equiv of bismuth(III) dimethylamide according to Scheme 1. After addition of the bismuth reagent,

Scheme 1. Synthesis of 2

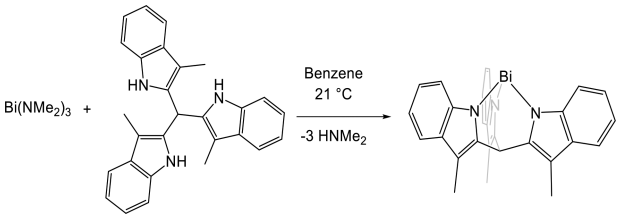

the colorless suspension turned into an orange homogeneous solution (see Figure S1). Solvent was removed under vacuum, and the recovered orange solid was suspended in anhydrous hexanes, vacuum filtered, and then dried under vacuum in an inert atmosphere. This product was fully characterized by different spectroscopic methods (for more information see SI). Unlike with **1**, no single crystals of **2** were obtained; however, loss of NH signal at 7.71 ppm in ^{1}H NMR (Figure S7) and its stretching frequency at 3398 cm^{-1} in FTIR (Figure S24) are consistent with the spectroscopic evidence established for **1** and support formation of **2**. Comparison of the ^{1}H NMR of **1** and **2** shows both compounds share similarities in integrated values with slight shifts on the chemical shifts of the protons in the solution. Additionally, the ^{13}C NMR chemical shifts and FTIR modes for compound **2** show similar features to compound **1**.

In the absence of crystallographic data, DFT calculations (B97-D3, def2-TZVPP, ZORA) were used to estimate the structural parameters of **2**. Atoms in molecules (AIM) analysis has proven to be a reliable method for evaluation of hydrogen bonding.[37,38] Recently, many studies have employed AIM analysis to evaluate the nature of noncovalent interactions. This method has proven its applicability for the evaluation of PnBs as well.[23,39,40]

Given the similarity in spectroscopic features, calculations were carried starting from the crystal structure of **1** by substituting a Bi in place of the Sb atom. The geometry optimizes to a C_{3v} symmetrical structure, consistent with calculations of **1**. The Bi−N bond lengths (2.168 Å) are close to previously reported Bi−N bond lengths for Bi compounds.[41−43] The electrostatic potential energy (ESP) (Figure 3) and the Fukui function integrated from above ($f^{+}(r)$) (See Figure S3) were separately mapped onto the electron density of **2** (0.001 au isosurface). Similar to **1**,[21] each maximum in the electrostatic potential (V_{max}) is located opposite to a Bi−N primary bond in a pocket created by the rigid cage motif and has a value of 187 kJ/mol. Each V_{max} overlaps with the regions predicted to be susceptible to nucleophilic attack according to the Fukui function (Figure S3). The V_{max} values are comparable with V_{max} values calculated on the 0.001 au molecular surface of strong neutral halogen (HaB) and chalcogen (ChB) bond donors that have been used for different purposes such as catalysis, molecular recognition, and anion recognition.[44−46]

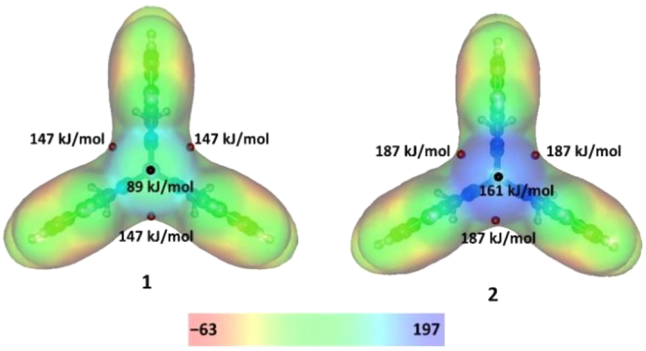

Figure 3. Electrostatic potential (ESP) maps of **1** (left) and **2** (right) on the electron density surface (0.001 au isosurface). Red and black spheres on ESP maps are locations of V_{max} and V_{min} respectively.

Compared to **1**, the potential associated with each V_{max} in **2** has increased by 40 kJ/mol. The value for the V_{min}, which is coincident with the pnictogen lone pair, displayed a more dramatic change. An increase of 72 kJ/mol compared with **1** is calculated, which is consistent with the increasing stereochemical inertness of the lone pair down the group.[32,47,48] It is important to note that sufficient anisotropy still remains in the electrostatic potential to direct the PnBs. Analysis of the frontier orbitals (HOMO−9) of **1** and **2** (illustrated in Figure S4) indicates the Bi lone pair orbital in **2** (−7.76 eV) is more energetically inaccessible than the Sb lone pair on **1** (−7.70 eV), consistent with the difference in the V_{min} values (Figure 3). This further serves to illustrate the role that the pnictogen lone pair plays in tuning the strength and directionality of the pnictogen bonding with trivalent molecules.[21,32] Another important factor is the increased size of Bi as compared to Sb. This Bi atom sits 1.358 Å above the plane that contains the three nitrogen atoms, compared with 1.251 Å for the Sb atom in **1**. This removal from the electron rich triskatylmethane will necessarily reduce the Pauli repulsion with an incoming PnB acceptor. Given the very promising electrostatic poential, the PnB ability was probed computationally by introducing pyridine (Py) molecules as PnB acceptors. The behavior of **2** was contrasted with **1** to determine if the introduction of Bi could mitigate the negative cooperativity that was previously observed when trying to achieve a triple pnictogen bond. An initial probe of negative cooperativity was performed by comparing the ESP maps of **2**·Py, **2**·Py_2, and **2**·Py_3. As shown in Figure 4, a decrease in the values of the remaining V_{max} and V_{min} occurs with each additional Py molecule. Notably, the decrease observed for **2** is not as steep as observed with **1** and the final V_{max} on **2**·Py_2 still has a value of 134 kJ/mol (ca. 53 kJ/mol in **1**·Py_2). Another feature of note is the residual electrostatic potential on **2**·Py_3 which is sufficiently large to allow an additional interaction.

To complement observations from the ESP maps and further understanding of the differences between addition of Py molecules to **1** and **2**, binding energies were evaluated (Table 1). The binding energy for the addition of the first pyridine molecule to **2** only differs by 8 kJ/mol compared to **1**. These values also indicate that the bonds fall in the strength regime of supramolecular interactions. The stepwise binding energy becomes an important consideration. Binding of the third Py molecule to **1** and **2** allows for the third stepwise binding energy to be determined and it highlights the critical difference between the two systems. In essence, once the

https://doi.org/10.1021/acs.inorgchem.1c01232
Inorg. Chem. XXXX, XXX, XXX−XXX

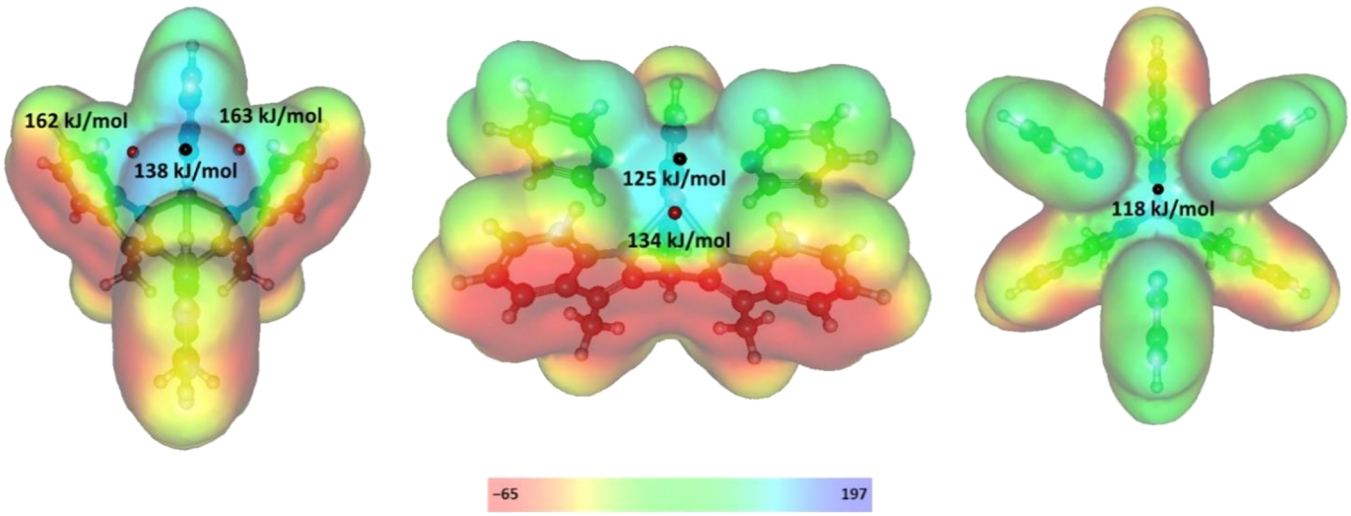

Figure 4. Electrostatic potential of **2**·Py (left), **2**·Py_2 (middle), and **2**·Py_3 (right) mapped onto the electron density surface (0.001 au isosurface). Position of V_{max} and V_{min} are indicated by red and black spheres and units are in kJ/mol.

Table 1. Binding Energy of Addition of 1-3 Py Molecules to 1 or 2[d]

	ΔE (kJ/mol)[a]		
	$n = 1$	$n = 2$	$n = 3$
1·Py_n[b]	−70	−136	−192
2·Py_n[c]	−78	−153	−220

[a]$\Delta E = \Delta E_{Binding} + \Delta E_{ZPE} + \Delta E_{BSSE}$. [b]**1** + n Py → **1**·Py_n. [c]**2** + n Py → **2**·Py_n. [d]**2**Energy units are in kJ/mol.

stepwise binding energy lies below a certain value, the probability of formation of the next PnB decreases. Here, it appears that dividing line is somewhere between −56 kJ/mol (**1**·Py_3 is not observed experimentally) and −66 kJ/mol (**2**·Py_3 is observed experimentally) for binding of Py to **1** and **2**. This indicates that **2**·Py_3 should be experimentally isolable in the solid state.

Binding to Pyridine. An orange suspension of **2**, in benzene, was treated with excess Py resulting in the formation of a clear yellow solution. Yellow block-shaped X-ray quality single crystals formed upon sitting at 21 °C for 24 h. The structure revealed that, in contrast to **1**, **2** can form three PnBs with three individual Py molecules in the solid state (Figure 5).

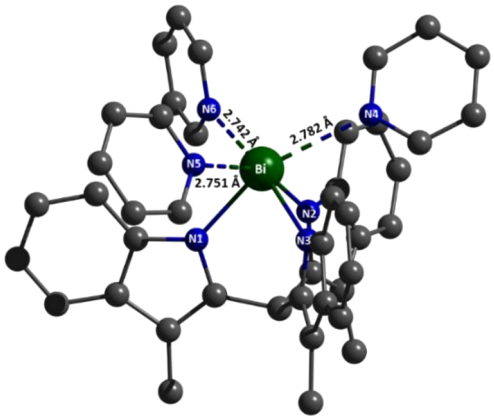

Figure 5. Ball and stick representation of **2**·Py_3. Hydrogen atoms and solvent molecules were omitted for clarity.

This is fully consistent with the DFT calculations (Table 2) and demonstrates the effectiveness of Bi over Sb in forming three simultaneous PnBs with pyridyl-based PnB acceptors . The Bi−N distances range from 2.217−2.235 Å. These are notably longer than those measured in the DFT model of **2**, but they are very well reproduced by the DFT model of **2**·Py_3. DFT models of with 1−3 pyridine molecules reveal that Bi−N bond elongation occurs opposite each PnB (Table 3). This is consistent with what has been previously observed in **1**·Py_3 and other pnictogen bonded systems.[21,31,32] Within an orbital model, this elongation can be rationalized by the population of a low-lying Bi−N σ^* orbital by the pyridine lone pair. The Bi··· N distances (Table 3) range from 2.742(2)-2.782(2) Å which are on average 76% of the $\sum r_{vdW}$.[49] These interactions are quite short yet still represent a 26% elongation over the Bi−N single bonds and are therefore clearly distinguished from typical single or strong coordination bonds. Compound $\mathbf{3}^{3+}$ was used as a point of comparison. On average, the Bi−N distances in $\mathbf{3}^{3+}$ were 111% of the $\sum r_{cov}$ of Bi and N.[50] Comparing this distance to the Bi···N distances of the supramolecules shows that they are shorter and closer to a covalent bond rather than a strong PnB. To further characterize the differences in the BiN bonding in these systems an AIM analysis was employed. Values for electron density (ρ), total electronic energy density (H),[51] and the $|V|/G$ indicator[52] at the bond critical points (BCP) of **2** supramolecules and $\mathbf{3}^{3+}$ are presented in Table 2. V refers to the electronic potential energy density (always negative) and G refers to the kinetic energy density (always positive). The value of the ρ at the BCP is related to the bond order for a given pair of atoms.[53] Comparison of the ρ values at BCPs for $\mathbf{3}^{3+}$ (0.0745 on average) showed that this value was 2.7 times larger than those calculated for the PnBs involving **2** (0.0273 on average), closer to the values for the Bi−N single bonds in **2**. This significant difference can be considered as an indication of greater covalency between Bi and N atoms in $\mathbf{3}^{3+}$. For **2**, addition of each subsequent Py molecule results in a slight decrease in the overall ρ at the PnB BCP, consistent with the changes in the ESP maps and the binding energies.

Bonds in which electrostatics dominate have values of $H > 0$ and $|V|/G < 1$ at the BCP.[51,52] A purely electrostatic model is often applied in order to rationalize the bonding in HaB, ChB,

https://doi.org/10.1021/acs.inorgchem.1c01232
Inorg. Chem. XXXX, XXX, XXX−XXX

Table 2. DFT Calculated Parameters and AIM Analysis of Coordination Compound 3^{3+}, 2 and Its Supramolecules

	2·Py	2·Py_2	2·Py_3	2·TPA	2·5[a]	2	3^{3+}
Bi−N (Å)	2.214	2.235	2.243	2.264	2.213	2.168	2.391
	2.189	2.241	2.243	2.271	2.224	2.168	2.305
	2.191	2.198	2.242	2.267	2.215	2.168	2.391
							2.305
Bi···N (Å)	2.772	2.836	2.847	2.867	2.882		
		2.807	2.846	2.889	2.801		
			2.846	2.808	2.737		
				3.064			
ρ (Bi−N, e $Å^{-3}$)						0.1043	0.0680
						0.1041	0.0810
						0.1042	0.0681
							0.0810
ρ (Bi···N, e $Å^{-3}$)	0.0313	0.0273	0.0269	0.0251	0.0253		
		0.0291	0.0270	0.0262	0.0290		
			0.0270	0.0289	0.0327		
				0.0192			
H (Bi−N)						−0.0347	−0.01475
						−0.0346	−0.02159
						−0.0347	−0.01477
							−0.02160
H (Bi···N)	−0.00149	−0.00071	−0.00060	−0.00040	−0.00029		
		−0.00104	−0.00063	−0.00056	−0.00092		
			−0.00061	−0.00101	−0.00164		
				0.00025			
$\lvert V\rvert/G$[b] (Bi−N)						1.393	1.301
						1.392	1.370
						1.392	1.301
							1.370
$\lvert V\rvert/G$[b] (Bi···N)	1.078	1.044	1.037	1.027	1.019		
		1.059	1.038	1.035	1.051		
			1.038	1.057	1.078		
				0.978			

[a]Only hydrogen positions were optimized, see Figure S5. [b]Calculated at Bi−N/Bi···N BCP.

Table 3. Bi−N and Bi···N Distances (Å) of the Supramolecules of 2

compound	$Bi-N_{1-3}$	$Bi\cdots N_n$
2·Py_3	$Bi-N_1$ 2.235(2)	$Bi\cdots N_4$ 2.782(2)
	$Bi-N_2$ 2.230(2)	$Bi\cdots N_5$ 2.742(2)
	$Bi-N_3$ 2.218(2)	$Bi\cdots N_6$ 2.751(2)
2·TPA	$Bi-N_1$ 2.264(4)	$Bi\cdots N_4$ 2.975(5)
	$Bi-N_2$ 2.253(4)	$Bi\cdots N_5$ 2.784(5)
	$Bi-N_3$ 2.248(5)	$Bi\cdots N_6$ 2.798(5)
		$Bi\cdots N_7$ 2.751(5)
2_2·4	$Bi-N_1$ 2.213(2)	$Bi\cdots N_4$ 2.737(2)
	$Bi-N_2$ 2.215(3)	$Bi\cdots N_5$ 2.801(2)
	$Bi-N_3$ 2.224(2)	$Bi\cdots N_6$ 2.751(2)

and PnB. Indeed, positive values for H are observed at the BCPs for halogen bonded systems.[54] It is important to note that the strength of the pnictogen bonds discussed here is much larger than those of typical halogen bonds. For the PnBs between **2** and Py, values of $H < 0$ and $|V|/G > 1$ are observed. The value of H is quite small and $|V|/G$ is close to 1, indicating that the role of covalency in stabilizing the interaction cannot be ignored. In contrast, values of $H = -0.01817$ and $|V|/G = 1.335$ (on average) were determined for 3^{3+} which supports significant covalency between Bi and N atoms, best described as strong coordinate covalent bonds. This compares well with the values for the covalent Bi−N primary bonds in **2**. These PnBs are weak coordination bonds, that lay in the strong regime of the named noncovalent interactions.[4]

Triple Pnictogen Bond Acceptors. The ability of **2** to simultaneously bind to three Py molecules through strong PnBs suggested that **2** could successfully form a triple PnB to tris(2-methylpyridine)amine (TPA), where **1** had failed.[21] Single crystals of **2** and TPA were grown by dissolving a 1:1 ratio of the two compounds in toluene. After sitting at room temperature (∼21 °C) for 24 h, yellow blade shaped X-ray quality single crystals of **2**·TPA were recovered and analyzed. The structure of **2**·TPA is depicted in Figure 6 and reveals that all three pyridyl groups of TPA formed short PnBs with **2** resulting in the anticipated triple PnB. The Bi···N PnB distances for the pyridyl groups ranged from 2.784 to 2.789 Å which is an average of 77% of the $\sum r_{vdW}$ and 127% of the $\sum r_{cov}$ of Bi and N. These distances are very similar to the ones found for **2**·Py_3 indicating a near perfect geometric match between the two units. An AIM analysis yields BCPs indicating presence of strong PnB along the $Bi\cdots N_{1-3}$ paths, with values of 0.0251−0.0289 e $Å^{-3}$ for the electron densities (ρ). Interestingly, a fourth short Bi···N distance is observed involving N_4. The distance is 82% of the $\sum r_{vdW}$ (136% $\sum r_{cov}$). While the electrostatic potential surface indicates that this could be a true attractive interaction, an AIM analysis was performed to evaluate the nature of this possible contact and

https://doi.org/10.1021/acs.inorgchem.1c01232
Inorg. Chem. XXXX, XXX, XXX−XXX

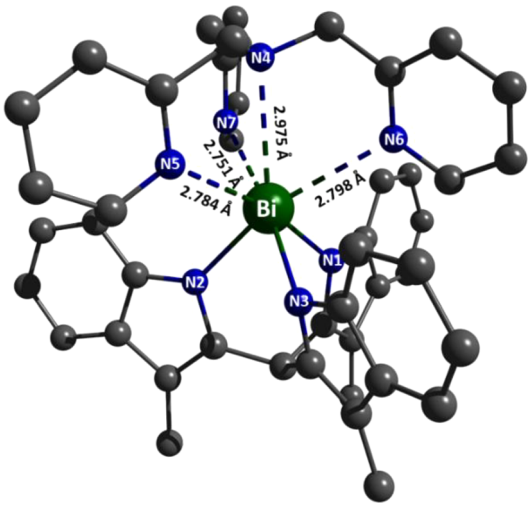

Figure 6. Ball and stick representation of **2**·TPA. Hydrogen atoms and solvent molecules are omitted for clarity.

indeed the electron density at the BCP was 0.0192 e $Å^{-3}$, which was sufficiently large that this could be considered as a medium to strong PnB. To further analyze the nature of this fourth interaction and probe the role that the constrained geometry of the TPA molecule plays, a model similar to **2**·TPA was chosen. This model (which will be denoted as **2**·Py_3·TMA) was developed from the geometry optimized **2**·Py_3 supramolecule where a trimethylamine (TMA) molecule was placed at a distance and similar position as the amine group in **2**·TPA. Energetics and AIM parameters were analyzed on the optimize **2**·Py_3·TMA (see Table S2 and S3). The final structure of **2**·Py_3·TMA appeared more distorted compared to **2**·TPA which appears to be the product of steric repulsion between the methyl groups on the TMA and the pyridine rings. An AIM analysis revealed an electron density of 0.0086 e $Å^{-3}$ at the BCP of Bi···N in between **2** and TMA which is consistent with a weak to medium PnB. Energy calculations also revealed a binding energy of −29 kJ/mol between **2**·Py_3 and TMA. This is smaller than the average binding energy for each Py molecule in **2**·Py_3 (−73.3 kJ/mol, Table 1). Overall, calculations suggested that even with loss of the rigidity in TPA Bi atom is still capable of forming a stabilizing interaction with a fourth N. This fourth PnB highlights the residual electrophilicity of the Bi atom even after it forms a triple PnB. We were curious if this would affect the self-assembly of the molecular capsule observed between **2** and the ditopic, tridentate PnB acceptor **4** that we had used previously to achieve a triple PnB with **1**.

Single crystals of $\mathbf{2}_2$·**4** were grown by mixing a 2:1 ratio of **2** and **4** in benzene and dissolving under mild heating. After the solution was stored at room temperature (∼21 °C) for 24 h, yellow octahedral-shaped crystals, suitable for single crystal diffraction, were formed. The crystal structure, depicted in Figure 7, shows that half of the atoms of $\mathbf{2}_2$·**4** were related to each other by a C_2 rotation axis. On average the Bi···N PnBs are 2.763 Å which is 77% of the $\sum r_{vdW}$ and 127% of the $\sum r_{cov}$ of Bi and N. In contrast to $\mathbf{1}_2$·**4**, a noticeable torsion between planes containing the arylethynyl arms of **4** and the central ring of **4**, was observed. Measurements revealed torsion angles between 22°−30° between these planes. Similar measurements were performed on $\mathbf{1}_2$·**4** and torsion angles were found to range between 1°−5°. As a result of the torsion, the Bi−Bi

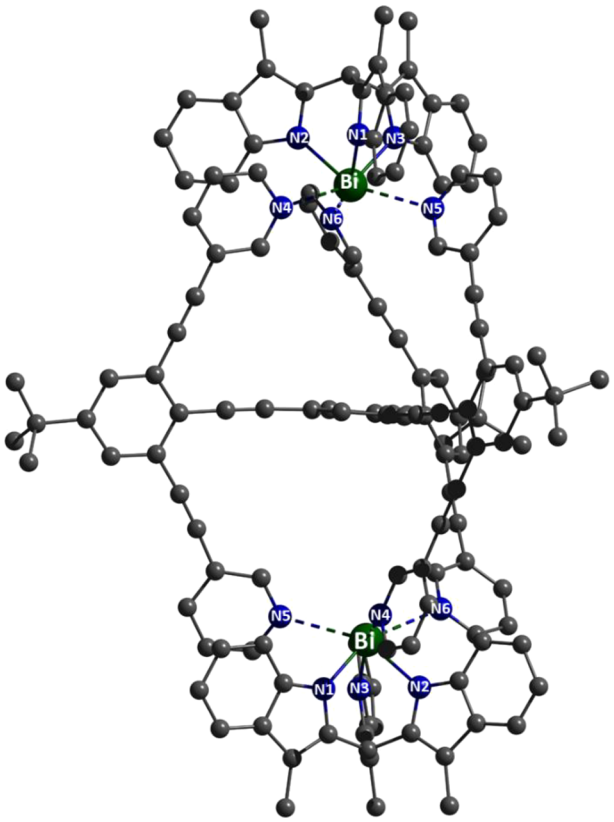

Figure 7. Ball and stick representation of $\mathbf{2}_2$·**4**. Hydrogen atoms and solvent molecules are omitted for clarity.

distance in $\mathbf{2}_2$·**4** is 0.428 Å shorter than the average Sb−Sb distance in (α and β)-$\mathbf{1}_2$·**4**. Similar to $\mathbf{1}_2$·**4**, two pseudotetrahedral cavities are formed in $\mathbf{2}_2$·**4**. In the structure, benzene molecules penetrate inside the cavities, but the small aperture appears to prevent the solvent molecules from becoming completely encapsulated. Like **2**·Py_3 and **2**·TPA, AIM analysis was performed on one-half of $\mathbf{2}_2$·**4** supramolecule denoted as **2**·**5** (see Figure S5). The large size, and corresponding computational demand required the use of this truncated model. The values at the bond critical points were in-line with those observed for **2**·Py_3 and **2**·TPA.

Pulsed-field Gradient Spin Echo (PFGSE) NMR (^{1}H) Spectroscopy. To study the integrity and behavior of the supramolecules in the solution state, diffusion coefficients of **2**, **2**·Py_3, **2**·TPA, and $\mathbf{2}_2$·**4** were studied via pulsed-field gradient spin echo (PFGSE) ^{1}H NMR spectroscopy in a benzene-d_6 solution. All diffusion coefficients were measured by fitting experimental values collected from PFGSE NMR experiments (for details, see S2.3 in the SI). In order to compare the values obtained from these experimental series, only the most intense nonoverlapping ^{1}H peaks (indicated in red in Figure 8) were analyzed. The diffusion coefficient of $\mathbf{2}_{Me}$ was 6.06×10^{-10} $m^2 \cdot s^{-1}$ (based on the methyl proton peak shown in Figure 8), and this value was used as a reference to follow the solution behavior of the supramolecules with **2**. A summary of the PFGSE NMR study is shown in Table 4. Using the Stokes−Einstein equation (see equation S2 in the SI) the Stokes radii (R_H) of **2** and the other supramolecules was evaluated (Table 4). A hydrodynamic volume (V_H) was determined by treating each species as spherical. These values were compared with the van der Waals volumes (V_{vdW}) estimated from the crystal

https://doi.org/10.1021/acs.inorgchem.1c01232
Inorg. Chem. XXXX, XXX, XXX−XXX

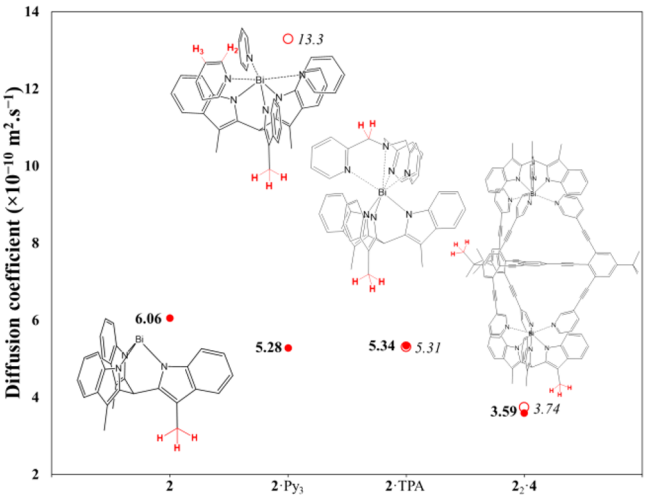

Figure 8. Diffusion coefficients measured in benzene-d6 solution of **2**, **2**·Py_3, **2**·TPA, $\mathbf{2}_2$·**4**. Solid markers represent diffusion coefficients fitted for protons of the methyl groups of **2** (bolded values on left side of the markers) and hollow dotted markers represent diffusion coefficients fitted for the most intense nonoverlapping proton signals of the pyridyl PnB acceptor molecules (italicized values on the right side of the markers).

Table 4. Chemical Shifts (δ), Diffusion Coefficients (D), and Stokes Radii (R_H) of 2, 2·Py_3, 2·TPA, and 2_2·4 Studied by PFGSE NMR Spectroscopy of ^{1}H Nuclei

Compound	δ (ppm)	D ($m^2.s^{-1}$)	R_H (nm)	V_H (Å^3)[a]	V_{vdW} (Å^3)[b]
$\mathbf{2}_{Me}$	2.51	6.06×10^{-10}	0.56	735	533[c]
$\mathbf{2}_{Me}$·Py_3	2.57	5.28×10^{-10}	0.73	1629	893
2·$Py_{3(H2)}$	8.18	13.2×10^{-10}	0.29	102	
2·$Py_{3(H3)}$	6.80	13.4×10^{-10}	0.29	102	
$\mathbf{2}_{Me}$·TPA	2.93	5.34×10^{-10}	0.63	1047	951
2·TPA_{Me}	3.46	5.31×10^{-10}	0.64	1097	951
$\mathbf{2}_{2(Me)}$·**4**	2.92	3.59×10^{-10}	1.07	5129	3680
2·$\mathbf{4}_{t\text{-}Bu}$	1.14	3.74×10^{-10}	1.03	4575	3680

[a]Hydrodynamic volume calculated based on measured R_H of each supramolecule. Volumes were calculated for a spheres. [b]van der Waals volume of each supramolecule based on subtraction of solvent molecule volume from the unit cell volume measured by X-ray diffraction. [c]Volume was calculated based on the crystal structure of **1**.

structure of each compound (the crystal structure of **1** was used as a surrogate for estimating the volume of **2**). The V_{vdW} of any interstitial solvents was subtracted to give the final tabulated values. It is essential to emphasize that the derived V_{vdW} should be expected to be smaller than V_H due to contraction at lower temperatures (100 K for crystal data collection) and lack of a solvation sphere.

As shown in Figure 8, the PFGSE characterization of **2**·Py_3 indicates a rapid exchange between **2** and Py molecules in the benzene-d_6 solution. The fitted value for proton peaks belonging to methyl groups of **2** ($\mathbf{2}_{Me}$·Py_3) in solution had a diffusion coefficient (5.28×10^{-10} $m^2 \cdot s^{-1}$) that was smaller compared to that of **2**. A larger diffusion coefficient was observed for the pyridine molecules in **2**·Py_3 (13.3×10^{-10} $m^2 \cdot s^{-1}$ on average). It is noteworthy to mention that the diffusion coefficient of benzene, which is similar in size with Py, is 16.8 $\times 10^{-10}$ $m^2 \cdot s^{-1}$. This is consistent with **2**·Py_3 being in equilibrium with free Py molecules. Meaningful comparison of V_H and V_{vdW} was not possible due to the presence of different species.

The solution behavior of **2**·TPA and $\mathbf{2}_2$·**4** were different compared to **2**·Py_3. Evaluation of the PFGSE NMR data revealed that all components of the supramolecules diffuse at similar rates in solution (Figure 8). The diffusion coefficient values obtained for **2**·TPA are very close to the value measured for $\mathbf{2}_{Me}$ in **2**·Py_3. This can be rationalized through the fact that both supramolecules are quite similar in size (Figure 6. The supramolecule $\mathbf{2}_2$·**4** is significantly larger than the other supramolecules that were investigated earlier, and it had the slowest rate of diffusion. The most important result of these experiments is the fact that both components of the supramolecules of **2**·TPA and $\mathbf{2}_2$·**4** diffuse together indicating that the equilibrium favors the self-assembled construct in the solution. Analysis of the V_H and V_{vdW} of both supramolecules (**2**·TPA and $\mathbf{2}_2$·**4**) shows a good correlation between the volumes of both compounds indicating that they are diffusing as aggregates that resemble those found in the crystal. This highlights the utility of employing a triple pnictogen bond for predictable molecular recognition and self-assembly, both in the solid state as well as in solution.

■ CONCLUSION

A new bismuth(III) PnB donor molecule was synthesized and characterized. The supramolecular chemistry was compared with the Sb congener, and it was found that the Bibased molecule can form three strong PnBs with a larger variety of PnB acceptors. This was established by solid-state and computational studies. Solution studies via PFGSE NMR spectroscopy showed that using more rigid PnB acceptor molecules can result in strongly interacting supramolecules that can keep their integrity in benzene solution. Lastly, analysis of the Bi PnBs reveal that they are highly directional but weak coordination bonds that support their categorization, in this case, as supramolecular interactions.

■ ASSOCIATED CONTENT

Supporting Information

The Supporting Information is available free of charge at https://pubs.acs.org/doi/10.1021/acs.inorgchem.1c01232.

Full synthetic procedures, characterization data, X-ray data analysis, computational methods, and diffusion NMR fits (PDF)

NMR jdf files (ZIP)

xyz coordinates (ZIP)

Accession Codes

CCDC 2073571−2073573 contain the supplementary crystallographic data for this paper. These data can be obtained free of charge via www.ccdc.cam.uk/data_request/cif, or by emailing data_request@ccdc.cam.uk, or by contacting The Cambridge Crystallographic Data Centre, 12 Union Road, Cambridge CB2 1 EZ, UK; fax: + 44 1223 336033.

■ AUTHOR INFORMATION

Corresponding Authors

Anthony F. Cozzolino − *Department of Chemistry and Biochemistry, Texas Tech University, Lubbock, Texas 79409-1061, United States;* orcid.org/0000-0002-1100-0829; Email: anthony.f.cozzolino@ttu.edu

Nathan P. Bowling − *Department of Chemistry, University of Wisconsin—Stevens Point, Stevens Point, Wisconsin 54481,*

https://doi.org/10.1021/acs.inorgchem.1c01232
Inorg. Chem. XXXX, XXX, XXX−XXX

United States; orcid.org/0000-0002-6930-1333; Email: nbowling@uwsp.edu

Authors

Shiva Moaven − *Department of Chemistry and Biochemistry, Texas Tech University, Lubbock, Texas 79409-1061, United States;* orcid.org/0000-0002-9846-2961

Brandon T. Watson − *Department of Chemistry and Biochemistry, Texas Tech University, Lubbock, Texas 79409-1061, United States*

Thomas J. Polaske − *Department of Chemistry, University of Wisconsin—Stevens Point, Stevens Point, Wisconsin 54481, United States*

Brian M. Karl − *Department of Chemistry, University of Wisconsin—Stevens Point, Stevens Point, Wisconsin 54481, United States*

Daniel K. Unruh − *Department of Chemistry and Biochemistry, Texas Tech University, Lubbock, Texas 79409-1061, United States;* orcid.org/0000-0002-2594-5786

Complete contact information is available at: https://pubs.acs.org/10.1021/acs.inorgchem.1c01232

Author Contributions

The manuscript was written through contributions of all authors. All authors have given approval to the final version of the manuscript.

Notes

The authors declare no competing financial interest.

■ ACKNOWLEDGMENTS

TTU group would like to acknowledge research funding (CHE 1847878) and instrument funding (NMR: CHE 1048553) from the National Science Foundation. The UWSP group would like to acknowledge research funding (CHE 1903581 and CHE 1606558) and instrument funding (NMR: CHE 0957080) from the National Science Foundation and research funding from the Henry Dreyfus Teacher-Scholar Awards Program.

■ REFERENCES

(1) Alcock, N. W. Secondary Bonding to Nonmetallic Elements. *Adv. Inorg. Chem. Radiochem.* **1972**, *15*, 1−58.

(2) Cozzolino, A. F.; Elder, P. J. W.; Vargas-Baca, I. A Survey of Tellurium-Centered Secondary-Bonding Supramolecular Synthons. *Coord. Chem. Rev.* **2011**, *255* (11−12), 1426−1438.

(3) Pitt, M. A.; Johnson, D. W. Main Group Supramolecular Chemistry. *Chem. Soc. Rev.* **2007**, *36* (9), 1441−1453.

(4) Cavallo, G.; Metrangolo, P.; Pilati, T.; Resnati, G.; Terraneo, G. Naming Interactions from the Electrophilic Site. *Cryst. Growth Des.* **2014**, *14* (6), 2697−2702.

(5) Desiraju, G. R.; Ho, P. S.; Kloo, L.; Legon, A. C.; Marquardt, R.; Metrangolo, P.; Politzer, P.; Resnati, G.; Rissanen, K. Definition of the Halogen Bond (IUPAC Recommendations 2013). *Pure Appl. Chem.* **2013**, *85* (8), 1711−1713.

(6) Aakeroy, C. B.; Bryce, D. L.; Desiraju, G. R.; Frontera, A.; Legon, A. C.; Nicotra, F.; Rissanen, K.; Scheiner, S.; Terraneo, G.; Metrangolo, P.; Resnati, G. Definition of the Chalcogen Bond (IUPAC Recommendations 2019). *Pure Appl. Chem.* **2019**, *91* (11), 1889−1892.

(7) Pascoe, D. J.; Ling, K. B.; Cockroft, S. L. The Origin of Chalcogen-Bonding Interactions. *J. Am. Chem. Soc.* **2017**, *139* (42), 15160−15167.

(8) Qiu, J.; Unruh, D. K.; Cozzolino, A. F. Design, Synthesis, and Structural Characterization of a Bisantimony(III) Compound for Anion Binding and the Density Functional Theory Evaluation of Halide Binding through Antimony Secondary Bonding Interactions. *J. Phys. Chem. A* **2016**, *120* (46), 9257−9269.

(9) Qiu, J.; Song, B.; Li, X.; Cozzolino, A. F. Solution and Gas Phase Evidence of Anion Binding through the Secondary Bonding Interactions of a Bidentate Bis-Antimony(III) Anion Receptor. *Phys. Chem. Chem. Phys.* **2018**, *20* (1), 46−50.

(10) Lee, L. M.; Tsemperouli, M.; Poblador-Bahamonde, A. I.; Benz, S.; Sakai, N.; Sugihara, K.; Matile, S. Anion Transport with Pnictogen Bonds in Direct Comparison with Chalcogen and Halogen Bonds. *J. Am. Chem. Soc.* **2019**, *141* (2), 810−814.

(11) Christianson, A. M.; Gabbaï, F. P. A Lewis Acidic, π-Conjugated Stibaindole with a Colorimetric Response to Anion Binding at Sb(III). *Organometallics* **2017**, *36* (16), 3013−3015.

(12) Park, G.; Brock, D. J.; Pellois, J.-P.; Gabbaï, F. P. Heavy Pnictogenium Cations as Transmembrane Anion Transporters in Vesicles and Erythrocytes. *Chem.* **2019**, *5* (8), 2215−2227.

(13) Gini, A.; Paraja, M.; Galmés, B.; Besnard, C.; Poblador-Bahamonde, A.; Sakai, N.; Frontera, A.; Matile, S. Pnictogen-Bonding Catalysis: Brevetoxin-Type Polyether Cyclizations. *Chem. Sci.* **2020**, *11* (27), 7086−7091.

(14) Hao, X.; Li, T.-R.; Chen, H.; Gini, A.; Zhang, X.; Rosset, S.; Mazet, C.; Tiefenbacher, K.; Matile, S. Bioinspired Ether Cyclizations within a π-Basic Capsule Compared to Autocatalysis on π-Acidic Surfaces and Pnictogen-Bonding Catalysts. *Chem. − Eur. J.* **2021**, 548 DOI: 10.1002/chem.202101548.

(15) Paraja, M.; Gini, A.; Sakai, N.; Matile, S. Pnictogen-Bonding Catalysis: An Interactive Tool to Uncover Unorthodox Mechanisms in Polyether Cascade Cyclizations. *Chem. - Eur. J.* **2020**, *26* (67), 15471−15476.

(16) Yang, M.; Hirai, M.; Gabbaï, F. P. Phosphonium−Stibonium and Bis-Stibonium Cations as Pnictogen-Bonding Catalysts for the Transfer Hydrogenation of Quinolines. *Dalton Trans.* **2019**, *48* (20), 6685−6689.

(17) Zhang, J.; Wei, J.; Ding, W.-Y.; Li, S.; Xiang, S.-H.; Tan, B. Asymmetric Pnictogen-Bonding Catalysis: Transfer Hydrogenation by a Chiral Antimony(V) Cation/Anion Pair. *J. Am. Chem. Soc.* **2021**, *143* (17), 6382−6387.

(18) Moaven, S.; Yu, J.; Vega, M.; Unruh, D. K.; Cozzolino, A. F. Self-Assembled Reversed Bilayers Directed by Pnictogen Bonding to Form Vesicles in Solution. *Chem. Commun.* **2018**, *54* (64), 8849−8852.

(19) Moaven, S.; Watson, B. T.; Thompson, S. B.; Lyons, V. J.; Unruh, D. K.; Casadonte, D. J.; Pappas, D.; Cozzolino, A. F. Self-Assembly of Reversed Bilayer Vesicles through Pnictogen Bonding: Water-Stable Supramolecular Nanocontainers for Organic Solvents. *Chem. Sci.* **2020**, *11* (17), 4374−4380.

(20) Mokrai, R.; Barrett, J.; Apperley, D. C.; Batsanov, A. S.; Benkő, Z.; Heift, D. Weak Pnictogen Bond with Bismuth: Experimental Evidence Based on Bi−P Through-Space Coupling. *Chem. - Eur. J.* **2019**, *25* (16), 4017−4024.

(21) Moaven, S.; Andrews, M. C.; Polaske, T. J.; Karl, B. M.; Unruh, D. K.; Bosch, E.; Bowling, N. P.; Cozzolino, A. F. Triple-Pnictogen Bonding as a Tool for Supramolecular Assembly. *Inorg. Chem.* **2019**, *58* (23), 16227−16235.

(22) Scilabra, P.; Terraneo, G.; Daolio, A.; Baggioli, A.; Famulari, A.; Leroy, C.; Bryce, D. L.; Resnati, G. 4,4′-Dipyridyl Dioxide·SbF3 Cocrystal: Pnictogen Bond Prevails over Halogen and Hydrogen Bonds in Driving Self-Assembly. *Cryst. Growth Des.* **2020**, *20* (2), 916−922.

(23) Mokrai, R.; Barrett, J.; Apperley, D. C.; Benkő, Z.; Heift, D. Tweaking the Charge Transfer: Bonding Analysis of Bismuth(III) Complexes with a Flexidentate Phosphane Ligand. *Inorg. Chem.* **2020**, *59* (13), 8916−8924.

(24) Anderson, K. M.; Baylies, C. J.; Jahan, A. H. M. M.; Norman, N. C.; Orpen, A. G.; Starbuck, J. Coordination Complexes of the Bismuth(III) Thiolates Bi(SC6F5)3 and Bi(SC6Cl5)3 with Pyridine Ligands. *Dalton Trans.* **2003**, No. 16, 3270−3277.

(25) Willey, G. R.; Daly, L. T.; Rudd, M. D.; Drew, M. G. B. Azamacrocyclic Complexation of Bismuth(III): Formation and

Structure of Fac-(BiCl3·Me3[9]AneN3) Where Me3[9]AneN3 = 1,4,7-Trimethyl-1,4,7-Triazacyclononane. *Polyhedron* **1995**, *14* (2), 315−318.

(26) Chitnis, S. S.; Burford, N.; Decken, A.; Ferguson, M. J. Coordination Complexes of Bismuth Triflates with Tetrahydrofuran and Diphosphine Ligands. *Inorg. Chem.* **2013**, *52* (12), 7242−7248.

(27) Chitnis, S. S.; Robertson, A. P. M.; Burford, N.; Patrick, B. O.; McDonald, R.; Ferguson, M. J. Bipyridine Complexes of E3+ (E = P, As, Sb, Bi): Strong Lewis Acids, Sources of E(OTf)3 and Synthons for EI and EV Cations. *Chem. Sci.* **2015**, *6* (11), 6545−6555.

(28) Sanderson, R. *Chemical Bonds and Bonds Energy*; Elsevier: 2012.

(29) Desiraju, G. R.; Steiner, T. *The Weak Hydrogen Bond: In Structural Chemistry and Biology*; Oxford University Press: 2001.

(30) Dolgonosov, A. M. The Universal Relationship between the Energy and Length of a Covalent Bond Derived from the Theory of Generalized Charges. *Russ. J. Inorg. Chem.* **2017**, *62* (3), 344−350.

(31) Moaven, S.; Yu, J.; Yasin, J.; Unruh, D. K.; Cozzolino, A. F. Precise Steric Control over 2D versus 3D Self-Assembly of Antimony(III) Alkoxide Cages through Strong Secondary Bonding Interactions. *Inorg. Chem.* **2017**, *56* (14), 8372−8380.

(32) Trubenstein, H. J.; Moaven, S.; Vega, M.; Unruh, D. K.; Cozzolino, A. F. Pnictogen Bonding with Alkoxide Cages: Which Pnictogen Is Best? *New J. Chem.* **2019**, *43* (36), 14305−14312.

(33) Scheiner, S. Coordination of a Central Atom by Multiple Intramolecular Pnicogen Bonds. *Inorg. Chem.* **2020**, *59*, 9315.

(34) Mason, M. R.; Phulpagar, S. S.; Mashuta, M. S.; Richardson, J. F. Synthesis and Characterization of Chelating Triamide Complexes of Bismuth and Antimony. *Inorg. Chem.* **2000**, *39* (17), 3931−3933.

(35) Shutov, P. L.; Karlov, S. S.; Harms, K.; Tyurin, D. A.; Churakov, A. V.; Lorberth, J.; Zaitseva, G. S. Synthesis and Characterization of the First Azastibatranes and Azabismatranes. *Inorg. Chem.* **2002**, *41* (23), 6147−6152.

(36) Turner, L. E.; Davidson, M. G.; Jones, M. D.; Ott, H.; Schulz, V. S.; Wilson, P. J. Bis(Bismuth)Toluene Inverted-Sandwich Complex Supported by Aminetris(Phenoxide) Ligands. *Inorg. Chem.* **2006**, *45* (16), 6123−6125.

(37) Espinosa, E.; Molins, E.; Lecomte, C. Hydrogen Bond Strengths Revealed by Topological Analyses of Experimentally Observed Electron Densities. *Chem. Phys. Lett.* **1998**, *285* (3), 170−173.

(38) Parthasarathi, R.; Subramanian, V.; Sathyamurthy, N. Hydrogen Bonding without Borders: An Atoms-in-Molecules Perspective. *J. Phys. Chem. A* **2006**, *110* (10), 3349−3351.

(39) Lu, L.; Lu, Y.; Zhu, Z.; Liu, H. Pnictogen, Chalcogen, and Halogen Bonds in Catalytic Systems: Theoretical Study and Detailed Comparison. *J. Mol. Model.* **2020**, *26* (1), 16.

(40) Li, Y.; Meng, L.; Sun, C.; Zeng, Y. Organocatalysis by Halogen, Chalcogen, and Pnictogen Bond Donors in Halide Abstraction Reactions: An Alternative to Hydrogen Bond-Based Catalysis. *J. Phys. Chem. A* **2020**, *124* (19), 3815−3824.

(41) Nekoueishahraki, B.; Samuel, P. P.; Roesky, H. W.; Stern, D.; Matussek, J.; Stalke, D. Organobismuth(III) and Dibismuthine Complexes Bearing N,N′-Disubstituted 1,8-Diaminonaphthalene Ligand: Synthesis, Structure, and Reactivity. *Organometallics* **2012**, *31* (18), 6697−6703.

(42) Schwamm, R. J.; Lein, M.; Coles, M. P.; Fitchett, C. M. Bi−P Bond Homolysis as a Route to Reduced Bismuth Compounds and Reversible Activation of P4. *Angew. Chem., Int. Ed.* **2016**, *55* (47), 14798−14801.

(43) Schwamm, R. J.; Coles, M. P.; Fitchett, C. M. Neutral and Cationic Bismuth Compounds Supported by Bis(Amidodimethyl)-Disiloxane Ligands. *Dalton Trans.* **2017**, *46* (12), 4066−4074.

(44) Benz, S.; Poblador-Bahamonde, A. I.; Low-Ders, N.; Matile, S. Catalysis with Pnictogen, Chalcogen, and Halogen Bonds. *Angew. Chem., Int. Ed.* **2018**, *57* (19), 5408−5412.

(45) Lohrman, J. A.; Deng, C.-L.; Shear, T. A.; Zakharov, L. N.; Haley, M. M.; Johnson, D. W. Methanesulfonyl-Polarized Halogen Bonding Enables Strong Halide Recognition in an Arylethynyl Anion Receptor. *Chem. Commun.* **2019**, *55* (13), 1919−1922.

(46) Biot, N.; Bonifazi, D. Concurring Chalcogen- and Halogen-Bonding Interactions in Supramolecular Polymers for Crystal Engineering Applications. *Chem. - Eur. J.* **2020**, *26* (13), 2904−2913.

(47) Pyykko, P. Relativistic Effects in Structural Chemistry. *Chem. Rev.* **1988**, *88* (3), 563−594.

(48) Lisac, K.; Topić, F.; Arhangelskis, M.; Cepić, S.; Julien, P. A.; Nickels, C. W.; Morris, A. J.; Friščić, T.; Cinčić, D. Halogen-Bonded Cocrystallization with Phosphorus, Arsenic and Antimony Acceptors. *Nat. Commun.* **2019**, *10* (1), 61.

(49) Mantina, M.; Chamberlin, A. C.; Valero, R.; Cramer, C. J.; Truhlar, D. G. Consistent van Der Waals Radii for the Whole Main Group. *J. Phys. Chem. A* **2009**, *113* (19), 5806−5812.

(50) Cordero, B.; Gómez, V.; Platero-Prats, A. E.; Revés, M.; Echeverría, J.; Cremades, E.; Barragán, F.; Alvarez, S. Covalent Radii Revisited. *Dalton Trans.* **2008**, No. 21, 2832−2838.

(51) Cremer, D.; Kraka, E. Chemical Bonds without Bonding Electron Density — Does the Difference Electron-Density Analysis Suffice for a Description of the Chemical Bond? *Angew. Chem., Int. Ed. Engl.* **1984**, *23* (8), 627−628.

(52) Espinosa, E.; Alkorta, I.; Elguero, J.; Molins, E. From Weak to Strong Interactions: A Comprehensive Analysis of the Topological and Energetic Properties of the Electron Density Distribution Involving X−H···F−Y Systems. *J. Chem. Phys.* **2002**, *117* (12), 5529−5542.

(53) Popelier, P. *Atoms in Molecules: An Introduction*; Prentice Hall: Essex, England, 2000.

(54) Ai-Guo, Z. Dissecting the Nature of Halogen Bonding Interactions from Energy Decomposition and Wavefunction Analysis. *Monatsh. Chem.* **2017**, *148* (7), 1259−1267.

https://doi.org/10.1021/acs.inorgchem.1c01232
Inorg. Chem. XXXX, XXX, XXX−XXX